IPN Progress Report 42-246 • August 15, 2026

Modeling Galactic Aberration Drift in VLBI

Alexander Tolstov,[*,§] Konstantin Belov,[*] Christopher Jacobs,[*] Gabor Lanyi,[*] and Charles Naudet[*]

ABSTRACT. — Galactic aberration drift (GAD), also commonly referred to as secular aberration drift (SAD), is the distance-independent dipolar proper-motion field of celestial objects induced by the long-term acceleration of the Solar System barycenter in the Milky Way potential [1, 2]. Although the effect is only a few microarcseconds per year, it accumulates over multi-decade very long baseline interferometry (VLBI) time spans and must be treated consistently to preserve the quasi-inertial character of the International Celestial Reference Frame (ICRF) [3, 4]. This article reviews the physical origin and expected sky signature of GAD, summarizes a vector-spherical-harmonic (VSH) formulation for representing low-degree proper-motion fields, and surveys the principal observational routes used to constrain the corresponding Galactic aberration constant, including Galactic-tracer astrometry, Gaia quasar astrometry, and extragalactic geodetic VLBI [3, 5]. Practical estimation strategies in VLBI (global multi-session versus session-wise/time-series approaches) are then discussed, with emphasis on robustness diagnostics required for microarcsecond-per-year global-mode recovery, given that individual-source apparent motions are frequently dominated by source-structure variability and other analysis-dependent systematics [3, 4]. Finally, the study identifies several practical directions for improving future GAD estimates: expanding southern-sky coverage, using controlled higher frequency multi-band observations as consistency checks, and maintaining more homogeneous long-term a priori products, including Earth-orientation inputs. These improvements would strengthen the estimation of GAD and would also benefit global geodetic products by ensuring that this deterministic low-order signal is treated consistently [3, 6].

---

[*] Deep Space Tracking Systems Section.

[§] Arizona State University.

The research described in this publication was carried out by the Jet Propulsion Laboratory, California Institute of Technology, under a contract with the National Aeronautics and Space Administration.

I. Introduction

The long-term acceleration of the Solar System barycenter toward the Milky Way center induces a slowly varying aberration effect that manifests as a systematic dipolar vector harmonics pattern in the apparent proper motions of distant extragalactic radio sources [1, 2, 7]. This phenomenon is referred to here as Galactic aberration drift (GAD) [7].

Recent geodetic very long baseline interferometry (VLBI) determinations and the International VLBI Service for Geodesy and Astrometry (IVS) Working Group 8 (WG8) assessment place the GAD amplitude at the level of 5–6 μas yr^{-1}, with a recommended value of 5.8 μas yr^{-1} for applications using the third realization of the International Celestial Reference Frame (ICRF3) [3, 4]. Over multi-decade VLBI baselines, an unmodeled GAD dipole accumulates to an apparent displacement at the $\sim 10^2$ μas level (e.g., $\sim 174\mu$as over 30 years for 5.8 μas yr^{-1}) [3]. Maintaining the International Celestial Reference Frame (ICRF) as a quasi-inertial celestial reference frame thus requires GAD to be incorporated consistently when propagating source positions across epochs, either through an a priori aberration model or through an equivalent global parameterization in the adjustment [3, 4].

At microarcsecond-per-year precision, GAD cannot be reliably inferred from any single source; instead, a large ensemble of sources is required to build statistical significance and to average down systematic effects such as source-structure evolution, centroid wander, and other analysis-dependent errors [3, 4]. Accordingly, GAD is estimated as a coherent low-order mode across a global set of sources, and the robustness of the solution depends critically on factors such as sky coverage, source selection, weighting schemes, and outlier handling [3].

In addition to reviewing the theoretical and observational framework, this work presents an implementation of GAD within the MODel and ESTimate (MODEST) VLBI analysis software package [8] and validates its behavior at the level of VLBI observables. Using differential residual diagnostics, we demonstrate that the modeled signal produces projection-dependent and time-dependent structures consistent with the expected dipolar geometry, providing an observable-level validation independent of post-fit proper-motion estimation.

II. Physical Origin and Expected Sky Signature

This galactic aberration is a relativistic phenomenon whereby the apparent direction to a source depends on the observer's instantaneous velocity, producing a purely geometric shift even when the source is intrinsically stationary [1, 7]. For an observer in uniform rectilinear motion, the aberrational offset remains constant in time. When the observer accelerates, however, the velocity vector changes secularly, and the aberration correction becomes time-dependent. At current levels of astrometric precision (several μas/yr), this secular variation is observed as an apparent proper-motion field on the sky rather than as a static position offset [1].

On Galactic scales, the Solar System barycenter is not inertial: it follows a curved orbit in the Milky Way potential and therefore undergoes a small acceleration whose dominant component is directed approximately toward the Galactic center [2, 3]. This acceleration imprints a coherent apparent proper-motion pattern on distant extragalactic radio sources that is independent of source distance. In reference-frame applications, the effect is therefore a global, low-order systematic effect that must be modeled or estimated consistently over multi-decade VLBI observation set time spans in order to maintain the quasi-inertial character of the ICRF [1, 4].

Geometrically, the leading-order sky signature of GAD is dipolar. The apparent proper-motion vectors are purely tangential, lying in the local tangent plane, and are aligned along great circles toward the acceleration apex. The field vanishes at the apex and antapex and reaches its maximum magnitude at an angular separation of 90° from the apex, consistent with the characteristic $\sin\zeta$ dependence, where ζ is the angular separation between the source direction and the acceleration vector, which determines the amplitude of the induced proper motion [1, 2]. The expected dipole pattern can be represented either by an acceleration vector in celestial-frame Cartesian coordinates or by an equivalent degree-1 vector spherical harmonic (VSH) expansion [3, 5].

Accordingly, the robustness of GAD estimation depends strongly on sky coverage, source selection, weighting, and long-term homogeneity of analysis conventions, because these choices determine how cleanly a small global dipole can be extracted from a much larger apparent-motion background [3].

III. Mathematical Formulation

In this section we follow the vector derivation of GAD given by Kopeikin and Makarov [1], in which the apparent source direction is written in terms of the unit direction vector $\mathbf{K}$ and the observer (Solar System barycenter) velocity and acceleration.

A. Vector Aberration and the Secular Term

Let $\mathbf{K}$ be the *true* (geometric) unit vector from the barycenter to a distant source, and let $\mathbf{k(t)}$ be the *apparent* unit direction at epoch t. Let the barycenter have velocity $\mathbf{v(t)}$ in a non-rotating Galactocentric frame, with acceleration $\mathbf{a} \equiv \mathbf{dv/dt}$ that is approximately constant over the VLBI time span. To first order in v/c (neglecting $O((v/c)^2)$ terms), the special-relativistic aberration shift can be written in vector form as

$$\mathbf{k(t)} = \mathbf{K} + \frac{\mathbf{1}}{\mathbf{c}}\,\mathbf{K} \times \big(\mathbf{v(t)} \times \mathbf{K}\big), \tag{1}$$

where c is the speed of light [1]. Over multi-decade intervals, the barycenter velocity about a reference epoch t_0 is

$$\mathbf{v(t)} \approx \mathbf{v_0} + \mathbf{a(t - t_0)}, \tag{2}$$

which gives

$$\mathbf{k(t)} = \mathbf{K} + \frac{\mathbf{1}}{\mathbf{c}}\,\mathbf{K} \times \big(\mathbf{v_0} \times \mathbf{K}\big) + \frac{\mathbf{1}}{\mathbf{c}}\,\mathbf{K} \times \big(\mathbf{a} \times \mathbf{K}\big)\,(\mathbf{t} - \mathbf{t_0}). \tag{3}$$

The second term is the (approximately constant) aberration field due to $\mathbf{v_0}$, while the third term is the secular change driven by the acceleration $\mathbf{a}$ [1].

B. Induced Proper Motion and the $\sin\zeta$ Dependence

For extragalactic sources, secular parallax terms are negligible. Given that the sources used in VLBI are typically at distances of order Gpc, secular parallax effects are of order nanoarcseconds and can therefore be neglected. Differentiating Equation (3) then yields the apparent proper-motion field [1]

$$\boldsymbol{\mu} \equiv \frac{d\mathbf{k}}{dt} = \frac{1}{c}\,\mathbf{K} \times \big(\mathbf{a} \times \mathbf{K}\big). \tag{4}$$

Using the vector triple-product identity $\mathbf{x} \times (\mathbf{y} \times \mathbf{z}) = \mathbf{y}(\mathbf{x} \cdot \mathbf{z}) - \mathbf{z}(\mathbf{x} \cdot \mathbf{y})$ and $\mathbf{K} \cdot \mathbf{K} = \mathbf{1}$, we obtain

$$\boldsymbol{\mu} = \frac{1}{c}\left[\mathbf{a} - (\mathbf{a} \cdot \mathbf{K})\,\mathbf{K}\right]. \tag{5}$$

Equation (5) shows that GAD is the projection of $\mathbf{a}/\mathbf{c}$ onto the tangent plane orthogonal to $\mathbf{K}$; in particular $\boldsymbol{\mu} \cdot \mathbf{K} = \mathbf{0}$, so the field is purely tangential.

To make the angular dependence explicit, define the *acceleration apex direction* $\hat{\mathbf{a}} \equiv \mathbf{a}/|\mathbf{a}|$, and define ζ as the angular separation between the source direction and the acceleration vector:

$$\cos\zeta \equiv \hat{\mathbf{a}} \cdot \mathbf{K} \qquad \Longleftrightarrow \qquad \mathbf{a} \cdot \mathbf{K} = |\mathbf{a}|\cos\zeta. \tag{6}$$

The proper-motion magnitude follows from Equation (5):

$$\begin{aligned} |\boldsymbol{\mu}|^2 &= \frac{1}{c^2}\,|\mathbf{a} - (\mathbf{a} \cdot \mathbf{K})\mathbf{K}|^2 \\ &= \frac{1}{c^2}\left(|\mathbf{a}|^{\mathbf{2}} - (\mathbf{a} \cdot \mathbf{K})^{\mathbf{2}}\right) = \frac{|\mathbf{a}|^{\mathbf{2}}}{c^2}\left(1 - \cos^2\zeta\right) = \frac{|\mathbf{a}|^{\mathbf{2}}}{c^2}\sin^2\zeta, \end{aligned} \tag{7}$$

and therefore

$$|\boldsymbol{\mu}| = \frac{|\mathbf{a}|}{c}\,\sin\zeta. \tag{8}$$

This makes the dipolar sky signature explicit: The field vanishes at the apex and antapex ($\zeta = 0, \pi$) and reaches its maximum magnitude at $\zeta = 90^\circ$ [2].

It is also useful to define the conventional GAD amplitude (Galactic aberration constant) in angular units as

$$A_G \equiv \frac{|\mathbf{a}|}{c}, \tag{9}$$

so that Equation (8) becomes $|\boldsymbol{\mu}| = A_G \sin\zeta$.

Figure 1 summarizes the geometry of the tangent-plane projection described by Equations (5)–(8).

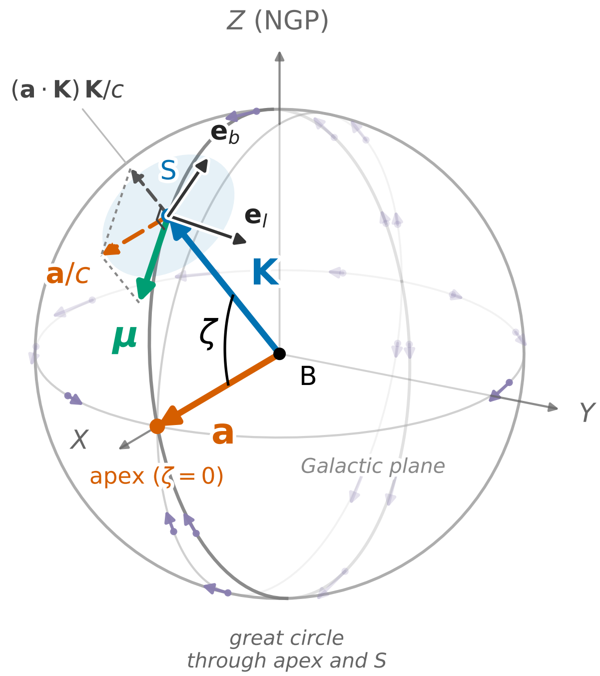

Figure 1. Geometry of Galactic aberration drift. The barycenter acceleration a defines the apex direction, and a source with unit direction K lies at angular separation ζ from that apex. The apparent proper motion $\boldsymbol{\mu}$ is the tangent-plane projection of $\mathbf{a}/c$ at the source direction, with magnitude $A_G \sin\zeta$. The field vanishes at the apex and antapex and reaches its maximum at $\zeta = 90°$.

C. Components in Galactic Longitude and Latitude

In Galactic spherical coordinates, defined by longitude l and latitude b, with associated tangent basis vectors $(\mathbf{e_l}, \mathbf{e_b})$, the proper-motion vector can be decomposed as $\boldsymbol{\mu} = \mu_l\,\mathbf{e_l} + \mu_\mathbf{b}\,\mathbf{e_b}$, where by convention $\mu_l \equiv \dot{l}\cos b$ and $\mu_b \equiv \dot{b}$ [1]. The Galactic coordinates (l, b) are obtained from the equatorial coordinates (α, δ) via the standard rotation from the International Celestial Reference System (ICRS) to the Galactic coordinate system [7]. Writing the acceleration vector as $\mathbf{a} = (\mathbf{a_X}, \mathbf{a_Y}, \mathbf{a_Z})$ in the Galactic Cartesian triad, the corresponding components of the proper-motion field are given by [1]

$$\mu_l = \frac{1}{c}\left(-a_X \sin l + a_Y \cos l\right), \tag{10}$$

$$\mu_b = \frac{1}{c}\left(-a_X \sin b \cos l - a_Y \sin b \sin l + a_Z \cos b\right). \tag{11}$$

D. Vector-Spherical-Harmonic Representation

A global proper-motion field $\boldsymbol{\mu}(\alpha, \delta)$ can be expanded into toroidal ("magnetic," $\mathbf{T}_{\ell\mathbf{m}}$) and spheroidal ("electric," $\mathbf{S}_{\ell\mathbf{m}}$) modes: [5]

$$\boldsymbol{\mu}(\alpha, \delta) = \sum_{\ell=1}^{\infty} \sum_{m=-\ell}^{\ell} \left[t_{\ell m}\,\mathbf{T}_{\ell\mathbf{m}}(\alpha, \delta) + \mathbf{s}_{\ell\mathbf{m}}\,\mathbf{S}_{\ell\mathbf{m}}(\alpha, \delta)\right]. \tag{12}$$

In this formalism, GAD is a lowest order ($\ell = 1$) *electric-type* field (spheroidal), fully described by the three independent components of $\mathbf{a}$ (equivalently the three $\ell = 1$ electric coefficients), whereas a residual global frame spin occupies the $\ell = 1$ *magnetic-type* (toroidal) subspace [3, 5].

In practical catalog and solution intercomparisons, the VSH expansion is often extended beyond $\ell = 1$ to test sensitivity to higher-order structure (e.g., quadrupole terms with $\ell = 2$). Uneven sky coverage and anisotropic source distributions can increase correlations among low-degree modes, allowing power to leak between dipole and quadrupole components if constraints and sampling are not handled carefully. This motivates reporting (or at least checking) low-degree mode covariance and stability under controlled changes in sky coverage and source selection in microarcsecond-per-year GAD analyses [3, 5]. Quadrupole terms are also of scientific interest because correlated quadrupolar patterns in apparent proper motions can be used to place astrometric bounds on a stochastic gravitational-wave background [9, 10].

IV. Estimation Strategies in VLBI: Global Multi-session Versus Session-wise Approaches

Because GAD is a low-order signal recovered statistically across many sources, its estimation depends strongly on solution strategy and constraints as well as on the underlying data volume. Two broad classes of approaches appear in the VLBI literature. In *global multi-session* solutions, the GAD dipole (or, equivalently, the acceleration vector) is estimated directly as a set of global parameters within a combined adjustment spanning many sessions. In *session-wise* (or time-series) approaches, source positions are estimated in individual sessions (or shorter time blocks), and GAD is subsequently inferred by fitting a dipole to the resulting source position time series or to per-source proper-motion estimates [2, 3].

A. Global Multi-Session Estimation

In a global adjustment, GAD parameters are introduced explicitly in the model (e.g., via an acceleration-vector parameterization) and are estimated simultaneously with other global quantities and nuisance parameters [3]. A primary advantage of this approach is that the covariance between GAD and other global degrees of freedom is handled self-consistently within a single normal-equation system. Global estimation also benefits from the full set of cross-session correlations implied by shared stations, networks, and consistent analysis conventions, which can reduce parameter scatter when the model and constraints are homogeneous over the analysis interval [3].

The principal limitation of global estimation is sensitivity to long-term inhomogeneity. Changes in network geometry, scheduling, data quality, analysis strategy, reference-frame realizations, and a priori products across decades can introduce small but coherent differences that project onto low-order patterns if they are not handled consistently. This does not imply that such effects mimic GAD deterministically; rather, it means that a single global adjustment can conflate multiple small contributions into the same fitted dipole component unless explicit diagnostics (e.g., time-splitting and convention checks) are performed [3, 4].

B. Session-wise and Time-Series Estimation

In session-wise approaches, source positions are estimated per session (or per shorter arc), and the resulting time series are used to infer proper motions or other summary statistics, after which a dipole model is fit to the ensemble [2]. This approach has two practical advantages. First, it supports localized diagnostics: sessions, sources, or epochs that behave anomalously can be identified and downweighted (or excluded) before fitting a global low-order model. Second, it allows direct visualization of time dependence, which can be useful for testing whether the inferred dipole is stable over the analysis interval or is driven by a limited subset of epochs. These features make session-wise strategies attractive for robustness studies and sensitivity analyses.

The corresponding drawback is statistical efficiency. Session-wise position estimates can be noisy for individual sources, and converting them into proper motions increases sensitivity to irregular sampling, outliers, and correlated errors. Moreover, fitting a dipole after the fact can obscure covariances with other global parameters unless the full error propagation is carried through consistently. As a consequence, session-wise strategies typically require careful weighting of per-source fits and stability filters to prevent a small number of highly variable sources from dominating the inferred dipole [3, 4].

C. Low-Degree Mode Separation and Sky-Sampling Considerations

In both global and session-wise frameworks, GAD is typically associated with the degree-1 electric-type component of the proper-motion field (or its equivalent acceleration-vector parameterization). In practice, analyses often examine additional low-degree modes (e.g., degree-1 magnetic-type global rotation and degree-2 quadrupole terms) to assess robustness and to test sensitivity to unmodeled large-scale structure [3, 5].

A key practical issue is that uneven sky coverage and anisotropic source distributions can increase correlations among low-degree modes. Incomplete southern-sky sampling, network-dependent observing patterns, or heavy downweighting of a subset of sources can bias the recovered dipole if power leaks between dipole and quadrupole components or if the dipole is partially absorbed by other global degrees of freedom. Accordingly, a defensible GAD analysis typically includes controlled tests in which the recovered degree-1 coefficients are checked for stability under changes in sky coverage, source selection, and low-degree model content (e.g., fitting $\ell = 1$ only versus fitting $\ell \leq 2$) [3, 5].

D. Longer Baselines, Sky Coverage, and Expected Improvement Over Time

For both approaches, increased data volume generally improves GAD recoverability. Longer time baselines reduce degeneracy between low-order modes and allow the dipole signal to accumulate relative to random scatter in session-wise estimates. In addition, improved sky coverage and a larger, more uniformly distributed source ensemble reduce sensitivity to anisotropic sampling and help decorrelate dipole parameters from other global degrees of freedom [3].

V. Implementation and Validation of Galactic Aberration Drift in MODEST

The MODEST VLBI analysis framework has been extended to support modeling of GAD, building on the standard geodetic and astrometric VLBI delay-modeling framework used in high-precision reference-frame analysis [8, 11]. In the present implementation, GAD is introduced as an optional model component, enabling controlled comparisons between solutions in which the model is disabled and those in which it is applied with varying amplitudes.

Rather than presenting a full estimation of the GAD amplitude, the focus here is on validating the implementation at the level of VLBI observables. The observed minus computed (O–C) diagnostics use paired MODEST runs on archived geodetic/astrometric VLBI sessions drawn from the IVS observing record. These sessions are part of the standard IVS geodetic observing program used for reference-frame, terrestrial-frame, and Earth-orientation analysis, rather than a special observing campaign designed specifically for GAD. The full all-session comparison therefore combines multiple IVS session types and observing geometries, including differences in station networks, baseline lengths and orientations, source lists, schedules, observing durations, and data volumes [3, 4]. For each paired comparison, the observation selection, a priori products, estimated parameters, and weighting strategy are held fixed; only the GAD model switch or assumed GAD amplitude is changed. The resulting differential residuals therefore isolate the observable-level response of the GAD correction, rather than representing an independent estimate of the GAD amplitude from a single session. This is accomplished through differential residual analysis, in which O–C group-delay residuals from solutions with GAD enabled are compared against a baseline solution in which the model is disabled:

$$\Delta(O-C) = (O-C)_{\text{model}} - (O-C)_{\text{OFF}}. \tag{13}$$

This differencing isolates the contribution of the GAD model and removes common-mode effects unrelated to the aberration signal, consistent with standard approaches to testing low-order global effects in VLBI solutions [3, 4].

This approach tests the GAD implementation directly at the level of VLBI observables, without relying on post-fit proper-motion estimation, and therefore provides an immediate validation of the model's physical consistency.

From the vector formulation (Section III), GAD produces a dipolar proper-motion field with magnitude proportional to $\sin\zeta$, where ζ is the angular separation between the source direction and the acceleration vector [1,2]. Accordingly, the induced residual response is expected to depend systematically on source direction and to exhibit a secular time dependence.

A. Projection-Based Validation (Single-Session Example)

To test the expected directional dependence, each observation is projected onto the Galactic acceleration direction. Figure 2 shows a representative example for the IVS geodetic VLBI session `10JAN04XA`, observed on 2010 January 4, in which $\Delta(O-C)$ is plotted as a function of the projection factor. This session is used as an observable-level implementation check: The goal is to verify that the modeled correction projects onto the group-delay residuals with the expected directional dependence, not to estimate a new GAD amplitude from this single session.

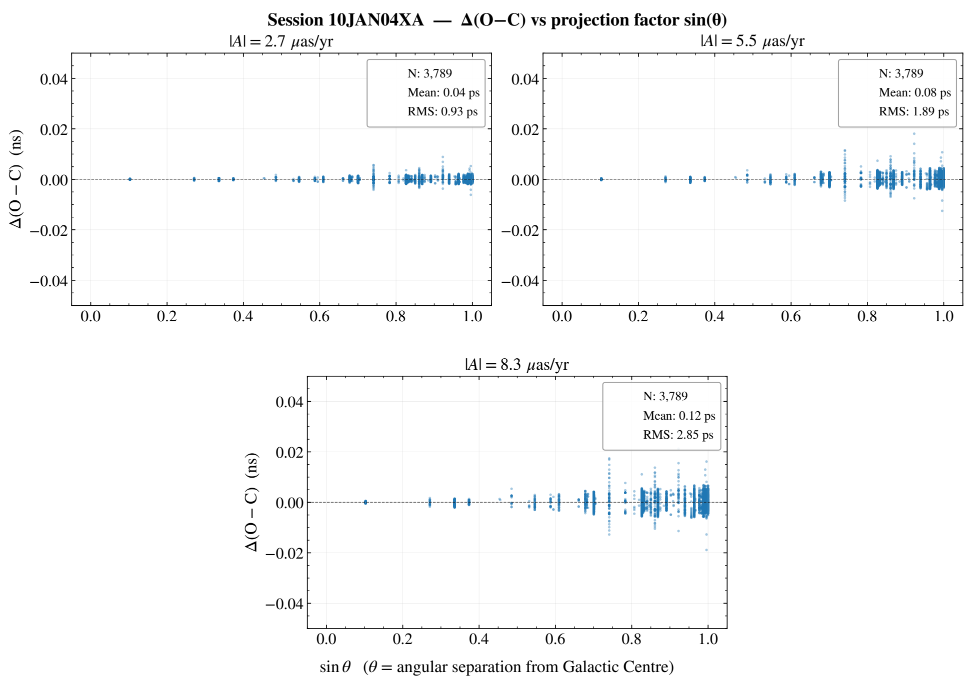

Figure 2. Differential residuals $\Delta(O-C)$ as a function of projection factor for session `10JAN04XA`, showing the directional dependence expected for the GAD dipole.

If the GAD implementation is correct, the differential residuals should exhibit a systematic dependence on projection, with structure consistent with the expected $\sin\zeta$ scaling of the dipole field. In the absence of a correctly implemented model, no such dependence would be expected and the distribution would remain statistically consistent with random scatter.

The key takeaway from this single-session diagnostic is the directional behavior of the residual difference, not a session-level determination of the GAD vector. The dependence of $\Delta(O-C)$ on the projection factor shows that the implemented correction enters the VLBI observables with the expected dipolar geometry. This provides a direct implementation check at the delay-observable level before any global source-motion or VSH estimation is attempted.

B. Time-Domain Validation Across Sessions

To assess temporal consistency, the same paired-run diagnostic is evaluated across the processed IVS geodetic/astrometric session set. Figure 3 shows $\Delta(O-C)$ as a function of observing time for a multi-decade collection, extending from 1995 to the recent IVS era. Because this collection combines many session types and network configurations rather than repeated observations of one fixed geometry, the time-domain response is expected to show a structured envelope with substantial session-to-session and observation-to-observation scatter.

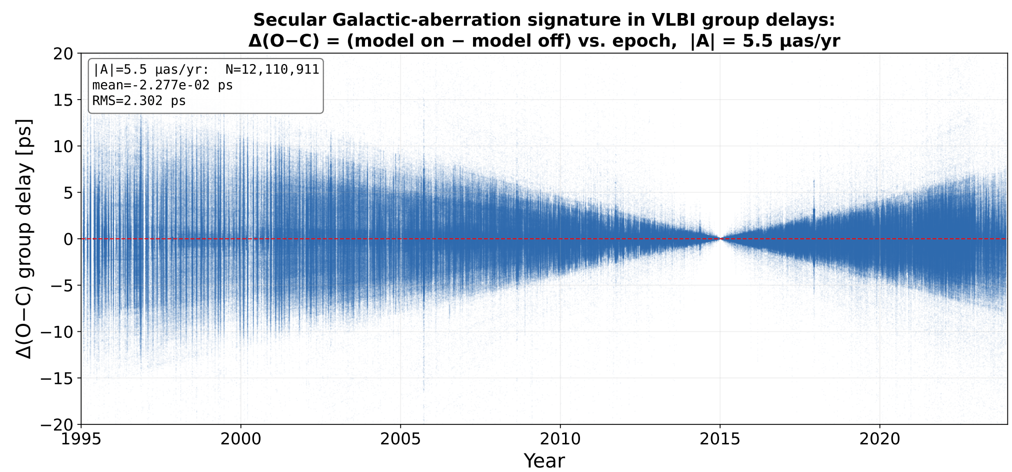

Figure 3. Differential residuals $\Delta(O-C)$ versus time across the processed IVS session set. The envelope widens away from the reference epoch as the GAD correction accumulates; scatter at fixed epoch reflects observation-dependent geometry.

The differential residuals exhibit a coherent temporal structure rather than purely random scatter, indicating that the model introduces a systematic correction consistent with the secular nature of GAD. The response is not expected to be a single-valued function of time. Schematically, the GAD contribution to an individual delay residual scales with both the elapsed time from the adopted reference epoch and an observation-dependent geometric factor,

$$\Delta\tau_i \propto (t_i - t_0)\, A_G\, G_i, \tag{14}$$

where G_i represents the projection of the GAD-induced source-direction change onto the particular source, baseline, and observing geometry for observation i. Thus, the envelope of the residual differences grows away from the reference epoch, while the vertical scatter at a given epoch is caused by differences in source direction, baseline orientation, station network, session schedule, observing duration, number of observations, and source distribution. The node near the adopted reference epoch (e.g., ICRF3 epoch ∼2015) reflects the convention that the GAD correction is applied as a time-dependent propagation relative to that epoch [3].

C. Sensitivity to Assumed GAD Amplitude

An additional validation of the implementation is obtained by varying the assumed amplitude of the GAD model and examining the resulting response in $\Delta(O-C)$. Figure 4 shows a representative example of the scaling of residual magnitude with assumed GAD amplitude.

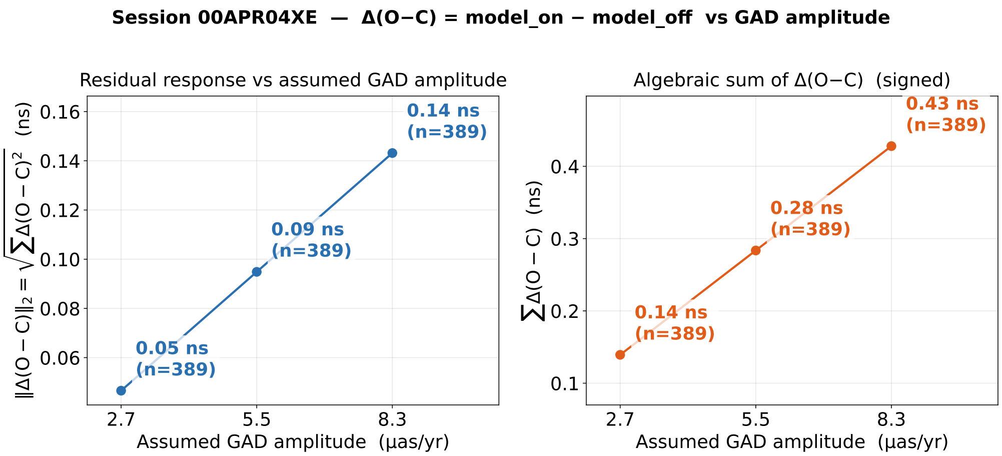

Figure 4. Residual response as a function of assumed GAD amplitude for session 00APR04XE. The approximately linear relationship provides an implementation check of the model scaling.

If the implementation is correct, the magnitude of the differential residuals should scale linearly with the assumed GAD amplitude. This behavior reflects the linear dependence of the model on the acceleration vector and provides an additional consistency check independent of sky geometry.

D. Interpretation

Taken together, these diagnostics provide an observable-level validation of the MODEST implementation of GAD. The presence of projection-dependent residual structure, its reproducibility across sessions, its coherent temporal behavior, and its linear scaling with assumed amplitude are all consistent with the expected tangential dipole field induced by Galactic acceleration.

In the VSH framework, this corresponds to the emergence of a degree-1 electric-type component in the proper-motion field [5].

These results indicate that the implemented model produces physically meaningful corrections at the level of VLBI delay observables, rather than purely numerical or stochastic effects. While this work does not attempt a full estimation of the GAD amplitude, it establishes a validated foundation for future global parameter estimation within the MODEST framework.

VI. External Observational Constraints on Galactic Aberration Drift

GAD[1] is commonly characterized by the Galactic aberration constant A_G, reported in angular units (e.g., $\mu\mathrm{as\,yr^{-1}}$) after conversion from $\mathrm{rad\,s^{-1}}$. In practice, constraints on A_G arise from complementary observational inputs: (i) measurements of *Galactic* tracers (masers) that constrain the local circular speed and Galactocentric distance and therefore the expected centripetal acceleration of the barycenter's orbit, and (ii) measurements of extragalactic astrometry that constrain the dipole component of the all-sky apparent proper-motion field directly [3].

A. Constraints from Galactic Tracer Astrometry (Masers)

High-precision astrometry of masers in star-forming regions provides trigonometric parallaxes and proper motions (often augmented by line-of-sight velocities). Interpreted within a Galactic rotation model, these measurements constrain the local circular speed V and Galactocentric distance R. These kinematic parameters set the expected centripetal acceleration scale of the barycenter's Galactic orbit, and the corresponding A_G follows from $|\mathbf{a}|/\mathbf{c}$ expressed in angular units. The older rows in Table 1 reproduce/adapt the IVS WG8 synthesis, while the newer rows provide recent Galactic-maser context using the same approximate conversion convention [3, 15, 16, 17, 18, 19, 20, 21].

B. Constraints from Extragalactic Astrometry in the Gaia Mission

The Gaia mission provides all-sky optical astrometry, including proper motions for large samples of compact extragalactic sources, primarily quasars or quasi-stellar objects (QSOs). In this framework, GAD is recovered as the degree-1 electric-type component of the proper-motion vector field via a VSH decomposition of the QSO proper motions [12, 13, 22].

In Gaia Data Release 2 (Gaia DR2), analysis of the Gaia Celestial Reference Frame 2 (Gaia-CRF2) showed that the fitted large-scale dipole-like term (denoted "glide" in the VSH formalism) is significant but is dominated by large-scale systematic effects in

---

[1] In the literature this same effect is commonly referred to as *secular aberration drift* (SAD), *Galactic aberration*, or the *acceleration of the Solar System barycenter*. See, e.g., VLBI-focused discussions of SAD/Galactic aberration and its reporting conventions, the ICRF3 implementation, Gaia's optical–quasi-stellar object (QSO) proper-motion determination of the Solar System acceleration, and reference-frame implications of Galactic aberration [1, 2, 3, 4, 12, 13, 14].

Table 1. GAD amplitude estimates from Galactic maser constraints on the circular speed V and Galactocentric distance R, converted via $V^2/(Rc)$. Rows through Rastorguev (2017) follow the IVS WG8 synthesis; for VERA (2020), V is derived from the published R and $\Omega_\odot$ [3,15,16,17,18,19,20,21]

.

Study	A_G [μas yr^{-1}]		V [km s^{-1}]		R [kpc]		# masers
	value	σ	value	σ	value	σ	
Reid (2009)	5.4	0.8	254	16	8.40	0.60	18
Brunthaler (2011)	5.1	0.8	246	7	8.30	0.23	18
Honma (2012)	4.9	0.6	238	14	8.05	0.45	52
Reid (2014)	4.8	0.3	240	8	8.34	0.16	103
Rastorguev (2017)	4.8	0.3	238	7	8.24	0.12	136
Reid (2019)	4.8	0.3	236	7	8.15	0.15	~200
VERA Collaboration (2020)	4.6	0.2	227	5	7.92	0.16	99

the DR2 proper motions, making DR2 unsuitable as a clean GAD measurement at the few-μas yr^{-1} level. By contrast, Gaia Early Data Release 3 (EDR3) enables a dedicated determination of the Solar System barycenter acceleration using ~1.2 million best-quality five-parameter QSO-like solutions and VSH fitting, yielding a dipole consistent with Galactic-potential expectations. Gaia-CRF3 provides the current Gaia DR3/EDR3 celestial reference-frame realization, but it should be treated as reference-frame context rather than as an independent new acceleration measurement because it uses the same basic astrometric solution as EDR3 [12, 13, 22].

Representative Gaia-based values are summarized in Table 2. Recent discussion of secular-aberration terms in stellar proper motions is useful context, but those stellar-catalogue papers should not be tabulated as new extragalactic-QSO GAD measurements [23, 24].

Table 2. Gaia-based constraints on GAD. Glide components (g_x, g_y, g_z) are in the ICRS; N_{QSO} is the number of QSO-like sources; dashes mark quantities that do not apply [12,13,22]

.

Gaia release	Quantity	Value [μas yr^{-1}]	Direction (RA, Dec) [deg]	N_{QSO}	Notes
Gaia DR2 (CRF2)	VSH glide	(−7.0, 4.7, 12.1)	146, +55	5.57×10^5	Systematics; away from GC
Gaia EDR3	GAD dipole	5.05 ± 0.35	269.1 ± 5.4 -31.6 ± 4.1	$\sim 1.2 \times 10^6$	Dedicated determination
Gaia DR3 (CRF3)	Frame realization	–	–	$\sim 1.6 \times 10^6$	Frame, not a measurement

C. Constraints from Extragalactic Astrometry in Geodetic VLBI

Geodetic VLBI constrains GAD using astrometry of compact extragalactic radio sources that define the ICRF [4]. In a multi-session VLBI analysis, apparent source motions (or, equivalently, low-order vector fields on the sky) may be inferred from source position time series or estimated directly through global dipole parameters. Within this framework, GAD appears as a degree-1 tangential dipole field. Published solutions differ in implementation details (e.g., whether the dipole direction is aligned a priori with the Galactic-center direction or estimated freely, and how source selection and weighting are handled), but the recovered amplitudes are broadly consistent at the level of a few $\mu\mathrm{as\,yr}^{-1}$ [3, 4]. Representative determinations are summarized in Table 3. Tables 1–3 summarize complementary constraints on the same physical acceleration at increasing levels of direct relevance to geodetic VLBI modeling. Table 1 gives Galactic-kinematic constraints from maser astrometry; these entries primarily constrain the expected GAD amplitude through the local circular speed and Galactocentric distance. Table 2 summarizes optical extragalactic constraints from Gaia QSO proper motions, including the fitted amplitude and direction where Gaia provides an independent acceleration estimate. Table 3 then gives the radio/VLBI determinations most directly comparable to this work, including observing span, amplitude, fitted dipole direction where available, and solution strategy. Together, the three tables show that independent observational routes consistently place GAD at the few-$\mu\mathrm{as\,yr}^{-1}$ level.

The consistency among the VLBI estimates in Table 3, together with the independent maser and Gaia constraints in Tables 1 and 2, supports treating GAD as a mostly known deterministic correction for routine geodetic VLBI processing. In this interpretation, single-session or limited-data-set solutions should generally apply an adopted GAD correction rather than attempt to estimate a new GAD vector independently. For a session-processing code path, this means that GAD is best treated as an a priori propagation correction in routine analysis, while revisions to the adopted GAD value should be obtained from dedicated global, long-time-span solutions with broad sky coverage, stable source selection, and controlled treatment of low-degree vector-field correlations.

D. Observational Content and Dominant Sensitivities

The three observational routes constrain the same physical quantity but with different dominant sensitivities, which is why the agreement across Tables 1–3 is useful. Maser-based determinations depend on the adopted Galactic rotation model and how the astrometric observables map to V and R. Gaia determinations constrain the dipole component of the all-sky extragalactic QSO proper-motion field in the optical via VSH fitting, with sensitivity dominated by large-scale astrometric systematics and source selection/quality cuts. VLBI determinations constrain the dipole field directly from radio astrometry, but are sensitive to reference-frame conventions, sky coverage,

Table 3. Geodetic VLBI estimates of GAD, as tabulated in the IVS WG8 synthesis [3] (original publications: [2, 25, 26, 27, 28]). A_G **is the component toward the Galactic center and RA/Dec give the apex direction. Calc/Solve global-solution uncertainties include a factor of 1.5 applied by WG8 to the formal errors.** $|A|$ **is computed from the WG8 Cartesian components, with its uncertainty taken as that of the dominant component** A_G**. Uncertainties are** 1σ**.**

Study	Span	A_G [μas yr^{-1}]	$\|A\|$ [μas yr^{-1}]	RA [deg]	Dec [deg]	Notes
Titov, Lambert, & Gontier (2011)	1990–2010	6.3 ± 0.9	6.4 ± 0.9	263 ± 11	-20 ± 12	Calc/Solve, time series
Titov & Lambert (2013)	1979–2013	6.4 ± 0.8	6.4 ± 0.8	266 ± 7	-26 ± 7	Calc/Solve, time series
Xu, Wang, & Zhao (2012)	1980–2011	5.2 ± 0.5	5.9 ± 0.5	243 ± 4	-11 ± 5	Calc/Solve, global
Xu (2017)[a]	1980–2016	6.0 ± 0.3	6.1 ± 0.3	271 ± 3	-21 ± 4	Calc/Solve, global
MacMillan (2014)	1979–2014	5.3 ± 0.4	5.6 ± 0.4	267 ± 4	-11 ± 6	Calc/Solve, global
MacMillan (2017)[a]	1979–2016	5.7 ± 0.3	5.8 ± 0.3	273 ± 3	-22 ± 5	Calc/Solve, global
Titov & Krásná (2018)	1979–2016	6.0 ± 0.3	6.1 ± 0.3	260 ± 2	-18 ± 4	VieVS, global
Titov & Krásná (2018)	1993–2016	5.4 ± 0.3	5.4 ± 0.3	273 ± 4	-27 ± 8	VieVS, global
Titov & Krásná (2018)	1979–2016	5.1 ± 0.2	5.2 ± 0.2	281 ± 3	-35 ± 3	VieVS, global/scale
WG8 recommended value	1979–2018	5.8 ± 0.3	5.9 ± 0.3	270 ± 3	-21 ± 5	Calc/Solve, global; ICRF3

Notes. Calc/Solve [29] and VieVS [30] are the Goddard and Vienna VLBI analysis packages. [a]Unpublished working-group solution reported in the WG8 synthesis [3]. MacMillan (2014) is documented in a conference abstract [27].

source selection, and non-stationarity of radio-source positions due to source structure [3, 4, 12, 13]. Thus, the main takeaway from Tables 1–3 is not that the measurements are redundant, but that independent observational routes converge on a consistent few-μas yr^{-1} effect. This supports use of an adopted GAD correction in routine processing, while motivating periodic re-estimation only in large, carefully controlled global analyses [3].

VII. Apparent Source Motions Versus the GAD Signal

GAD is expected to appear as a low-amplitude, degree-1 (dipole) tangential vector field on the celestial sphere, with a characteristic maximum magnitude of only a few μas yr^{-1} [2, 3]. In contrast, apparent motions inferred from VLBI source position time series are frequently dominated by non-GAD contributions, including source-structure evolution, centroid wander, and other analysis-dependent modeling and convention choices. Source structure is a well-known contributor to astrometric and geodetic

VLBI error budgets, and recent work continues to emphasize the need for source-quality assessment and source-structure-aware weighting in high-precision VLBI analysis [3, 4, 31, 32, 33]. Consequently, GAD is recovered as a coherent low-order mode only through estimation across a large ensemble of sources, and its robustness depends on source stability, sky coverage, weighting, and outlier handling [3, 4].

Figure 5 illustrates this observational context using an all-sky quiver representation of apparent proper-motion vectors derived from VLBI source astrometry. The field is heterogeneous: amplitudes and directions vary substantially from source to source, and local patterns can be dominated by a relatively small number of unstable objects. Such behavior is consistent with the fact that the leading contributors to apparent motion are often source-specific rather than a single global signal. Importantly, the presence of large, irregular apparent motions does not preclude GAD; it implies that GAD must be extracted as a weak, spatially coherent dipole component embedded within a much larger apparent-motion background [3, 4].

For comparison, Figure 6 shows a theoretical template of the GAD dipole field for a reference amplitude. In this idealized case, the vectors are purely tangential and exhibit a coherent dipolar structure: The field vanishes at the acceleration apex and antapex and reaches maximum magnitude near 90° angular separation [1, 2]. The qualitative difference between Figures 5 and 6 motivates formulating GAD estimation explicitly in a basis that targets low-order vector fields (e.g., an acceleration-vector parameterization or an $\ell = 1$ electric-type representation), rather than relying on individual source motions for interpretation [3, 5].

Two practical implications follow. First, sensitivity to GAD depends strongly on the stability of the source ensemble and on the adopted weighting and outlier-handling strategy, since a small fraction of sources with large structure-driven motions can project significantly onto low-order modes. Second, recoverability of a dipole field is conditioned on sky coverage: anisotropic source distributions or network-dependent observing patterns can increase covariance between the dipole and other global degrees of freedom and can amplify sensitivity to source selection. These considerations motivate explicit robustness diagnostics (e.g., stability-based source selection, time-splitting, and band-splitting consistency checks) as standard components of microarcsecond-per-year GAD analyses [3, 4].

VIII. Improvements and Forward-Looking Analysis Directions

Because GAD is a microarcsecond-per-year, low-order global mode, practical limitations are typically set by (i) the stability and sky distribution of the reference-source ensemble and (ii) the long-term homogeneity of analysis inputs and conventions across multi-decade VLBI time spans [3, 4]. The subsections below summarize forward-looking directions that can improve robustness of GAD estimation without changing the underlying physical interpretation of the signal.

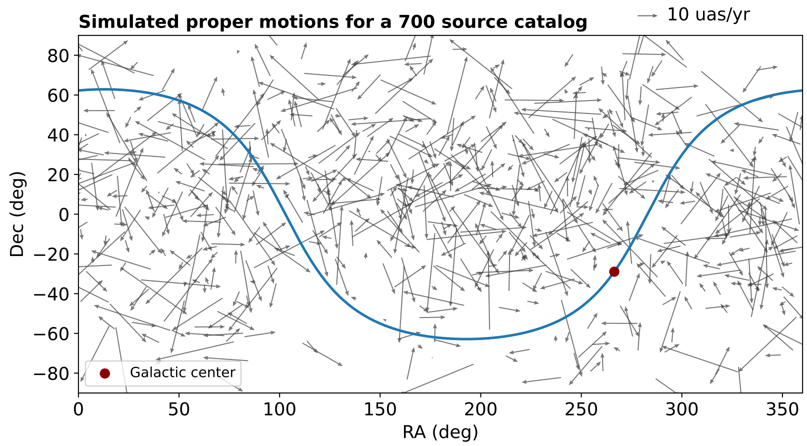

Figure 5. All-sky apparent proper-motion vector field from VLBI source astrometry (illustrative quiver plot). The heterogeneity in amplitude and direction reflects source-dependent apparent motions and analysis/systematic effects that dominate individual-source behavior.

A. Sky Coverage and Multi-Band Supplementation (S- and X-Bands with K-band and Related Data)

Geodetic VLBI GAD analyses are naturally anchored in S- and X-bands because they provide the longest and most homogeneous observing record and support dual-frequency mitigation of first-order ionospheric delay [4, 6]. Within this baseline, a primary improvement route is to increase the uniformity of all-sky constraints on low-order vector fields. Current astrometric coverage remains uneven, with a predominance of well-observed sources in the northern hemisphere. Such hemispheric imbalance can increase sensitivity of dipole estimates to source selection and to network geometry, because non-uniform sky sampling effectively weights some dipole components more strongly than others [3].

A complementary route is multi-band supplementation rather than band replacement. Higher-frequency VLBI observations, such as K-band at ~ 24 GHz, provide an independent astrometric data stream that can serve as a consistency diagnostic against frequency-dependent source structure and other band-dependent systematics. At K-band, the ionospheric delay is smaller because of the higher observing frequency; however, standalone K-band observations do not provide the same dual-frequency ionospheric calibrations available in standard S/X- or X/Ka-band combinations [6, 34]. The tradeoffs are also well known: Source flux densities are often lower at higher frequency, sky coverage may be less uniform, and the relative importance of tropospheric delay modeling tends to increase [4, 6]. Accordingly, the most defensible role of K-band in GAD work is as a controlled robustness check: A recovered dipole should remain stable (within expected uncertainty) under carefully managed changes in band, source selection, and weighting, while persistent band-dependent shifts should be interpreted conservatively as evidence of unmodeled frequency-dependent systematics projecting into low-order modes [3, 4].

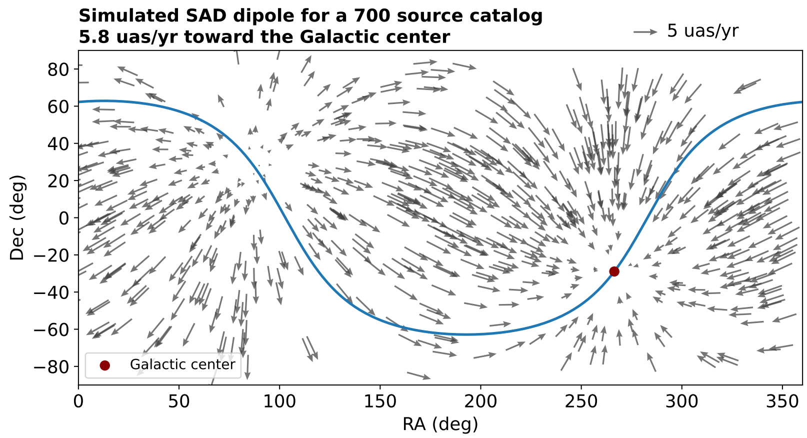

Figure 6. Idealized GAD dipole proper-motion field shown for a reference amplitude (illustrative template). The field is tangential and dipolar, with maximum magnitude near 90° from the acceleration apex and vanishing at the apex and antapex.

B. Improved a Priori Earth Orientation and Long-Term Homogeneity of Analysis Inputs

Independent of observing band, GAD estimation is vulnerable to long-term inhomogeneities that can project into the lowest order sky patterns. These include changes in a priori reference products and convention-level modeling choices applied across decades (e.g., Earth orientation parameter (EOP) series updates, terrestrial reference frame and celestial reference frame realization transitions, and model-option differences). Galactic-aberration modeling has also been shown to affect reference-frame realization and can couple into Earth-orientation-related analysis if treated inconsistently. Even when unrelated to GAD physically, small but coherent differences introduced at the observable or constraint level can bias an estimated dipole if they correlate with time and are not treated consistently across the full analysis span [3, 6, 35, 36]. A practical way to diagnose such sensitivities is to examine controlled solution differences in which only one model term is toggled. Figure 3 shows the differential observed minus computed (O–C) group-delay residuals between two otherwise identical solutions that differ only by inclusion of the GAD model. The difference exhibits a clear epoch dependence, with a node near the adopted reference epoch and a growing magnitude away from it, reaching amplitudes of order ± 10 ps (equivalently $\sim \pm 3$ mm in light-travel path length). This behavior is not interpreted as a geophysical signal; rather, it illustrates that deterministic convention-level choices can imprint structured residual patterns over multi-decade spans. In microarcsecond-per-year global-mode studies, such structure can leak into low-order parameter estimates unless the analysis is internally homogeneous and accompanied by explicit consistency checks [3, 4, 6].

More broadly, a priori EOP inputs provide another important pathway for long-term inhomogeneity. Regime changes in EOP products (processing updates, modeling changes, or transitions between reference realizations) can alter the noise statistics and introduce small discontinuities that are negligible for many applications but nontrivial for weak global signals. Figure 7 illustrates this general issue using a long time series of an EOP-related quantity (labeled ψ), where the statistical character changes across the observing interval. The figure is included as analysis context: The key point is that GAD studies benefit from explicit provenance tracking for a priori products, along with time-splitting and reprocessing tests whenever product updates or discontinuities are suspected [6, 37].

In practice, these considerations motivate a small set of standard robustness diagnostics: (i) Repeat the global fit under alternative, well-defined a priori EOP series; (ii) split the analysis into time blocks bracketing known product or network transitions; and (iii) compare the recovered dipole and other low-order modes across these controlled variants. Improved a priori inputs can reduce unmodeled structure that would otherwise project into low-order sky patterns, while consistent GAD treatment reduces the need for other estimated parameters to absorb a deterministic dipole contribution, supporting internal consistency of global VLBI products [3, 4].

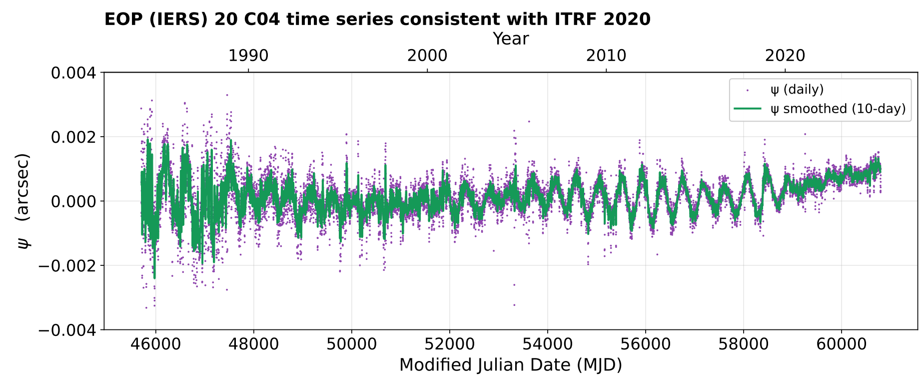

Figure 7. Illustrative long time series of an EOP-related quantity (ψ), shown to emphasize that changes in statistical character or processing regimes can motivate explicit provenance tracking and time-splitting checks in microarcsecond-per-year global-mode estimation. (Shown as analysis context; not interpreted as a GAD signature.)

IX. Conclusion

GAD is a deterministic, distance-independent dipolar proper-motion field arising from the Solar System barycenter's long-term Galactocentric acceleration [1]. Because the effect is only a few μas yr^{-1}, it becomes operationally relevant through accumulation over multi-decade VLBI time spans and through its projection into the lowest order global patterns used to realize and maintain the ICRF [3, 4].

The vector formulation provides a compact description of the induced proper-motion field and exposes the expected $\sin\zeta$ sky signature and purely tangential geometry [1]. The VSH representation provides a natural framework for expressing and comparing low-order vector fields on the celestial sphere, including separation of degree-1 electric-type dipole terms from global frame-spin modes [3, 5].

A practical implication emphasized by the WG8 synthesis is that GAD modeling is tied to an adopted reference epoch for convention-level propagation in modern reference-frame realizations. In ICRF3-era applications, a reference epoch near 2015 is commonly used, so analyses that do not explicitly model GAD may show smaller apparent impact close to that epoch but can accumulate increasing inconsistency away from it over multi-decade time spans [3, 4].

This work also demonstrates the implementation of Galactic aberration drift within the MODEST VLBI analysis framework and its validation at the level of VLBI delay observables. By comparing solutions with and without the GAD model, differential residual diagnostics reveal projection-dependent structure consistent with the expected $\sin\zeta$ dipole and a coherent temporal behavior with a node near the reference epoch. These results provide direct evidence that the implemented model produces physically meaningful corrections in VLBI observables, rather than purely numerical artifacts.

Looking forward, improved GAD robustness is primarily enabled by (i) a more uniform and stable reference-source ensemble (with particular attention to southern-sky coverage), (ii) controlled multi-band supplementation (e.g., K-band) as a consistency diagnostic against frequency-dependent source structure, and (iii) long-term homogeneity of a priori products and conventions, including Earth-orientation inputs, so that unrelated regime changes do not leak into the lowest order patterns [3, 4, 6].

References

[1] S. M. Kopeikin and V. V. Makarov, "Astrometric effects of secular aberration," *The Astronomical Journal*, vol. 131, no. 3, pp. 1471–1478, Mar. 2006.

[2] O. Titov, S. B. Lambert, and A.-M. Gontier, "VLBI measurement of the secular aberration drift," *Astronomy & Astrophysics*, vol. 529, p. A91, May 2011.

[3] D. S. MacMillan, A. Fey, J. M. Gipson, D. Gordon, C. S. Jacobs, H. Krásná, S. B. Lambert, Z. Malkin, O. Titov, G. Wang, and M. H. Xu, "Galactocentric acceleration in VLBI analysis. Findings of IVS WG8," *Astronomy & Astrophysics*, vol. 630, p. A93, 2019.

[4] P. Charlot, C. S. Jacobs, D. Gordon, S. Lambert, A. de Witt, J. Böhm, A. L. Fey, R. Heinkelmann, E. Skurikhina, O. Titov, E. F. Arias, S. Bolotin, G. Bourda, C. Ma, Z. Malkin, A. Nothnagel, D. Mayer, D. S. MacMillan, T. Nilsson, and R. Gaume, "The third realization of the International Celestial Reference Frame by very long baseline interferometry," *Astronomy & Astrophysics*, vol. 644, p. A159, Dec. 2020.

[5] F. Mignard and S. A. Klioner, "Analysis of astrometric catalogues with vector spherical harmonics," *Astronomy & Astrophysics*, vol. 547, p. A59, 2012.

[6] G. Petit and B. J. Luzum, Eds., *IERS Conventions (2010)*, ser. IERS Technical Note. Frankfurt am Main: Verlag des Bundesamts für Kartographie und Geodäsie, 2010, no. 36.

[7] J. Kovalevsky, "Aberration in proper motions," *Astronomy & Astrophysics*, vol. 404, pp. 743–747, Jun. 2003.

[8] O. J. Sovers and C. S. Jacobs, "Observation model and parameter partials for the JPL VLBI parameter estimation software MODEST, 1996," JPL Publication 83-39, rev. 6, 151 pages, p. 8339, Aug. 1996.

[9] C. R. Gwinn, T. M. Eubanks, T. Pyne, M. Birkinshaw, and D. N. Matsakis, "Quasar proper motions and low-frequency gravitational waves," *The Astrophysical Journal*, vol. 485, no. 1, pp. 87–91, 1997. https://doi.org/10.1086/304424

[10] J. Darling, A. E. Truebenbach, and J. Paine, "Astrometric limits on the stochastic gravitational wave background," *The Astrophysical Journal*, vol. 861, no. 2, p. 113, 2018. https://doi.org/10.3847/1538-4357/aac772

[11] O. J. Sovers, J. L. Fanselow, and C. S. Jacobs, "Astrometry and geodesy with radio interferometry: Experiments, models, results," *Reviews of Modern Physics*, vol. 70, no. 4, pp. 1393–1454, Oct. 1998.

[12] Gaia Collaboration, F. Mignard, S. A. Klioner, L. Lindegren, J. Hernández, U. Bastian, A. Bombrun, et al., "Gaia data release 2: The celestial reference frame (Gaia-CRF2)," *Astronomy & Astrophysics*, vol. 616, p. A14, 2018. https://doi.org/10.1051/0004-6361/201832916

[13] Gaia Collaboration, S. A. Klioner, F. Mignard, L. Lindegren, U. Bastian, P. J. McMillan, J. Hernández, D. Hobbs, et al., "Gaia early data release 3: Acceleration of the Solar System from Gaia astrometry," *Astronomy & Astrophysics*, vol. 649, p. A9, 2021. https://doi.org/10.1051/0004-6361/202039734

[14] Z. Malkin, "On the implications of the galactic aberration in proper motions for the celestial reference frame," *Monthly Notices of the Royal Astronomical Society*, vol. 445, no. 1, pp. 845–849, 2014. https://doi.org/10.1093/mnras/stu1796

[15] M. J. Reid, K. M. Menten, X. W. Zheng, A. Brunthaler, L. Moscadelli, Y. Xu, B. Zhang, et al., "Trigonometric parallaxes of massive star-forming regions. VI. Galactic structure, fundamental parameters, and noncircular motions," *The Astrophysical Journal*, vol. 700, no. 1, pp. 137–148, 2009. https://doi.org/10.1088/0004-637X/700/1/137

[16] A. Brunthaler, M. J. Reid, K. M. Menten, X.-W. Zheng, A. Bartkiewicz, Y. K. Choi, T. Dame, et al., "The bar and spiral structure legacy (BeSSeL) survey: Mapping the milky way with VLBI astrometry," *Astronomische Nachrichten*, vol. 332, no. 5, pp. 461–466, 2011. https://doi.org/10.1002/asna.201111560

[17] M. Honma, T. Nagayama, K. Ando, T. Bushimata, Y. K. Choi, T. Handa, T. Hirota, et al., "Fundamental parameters of the milky way galaxy based on VLBI astrometry," *Publications of the Astronomical Society of Japan*, vol. 64, no. 6, p. 136, 2012. https://doi.org/10.1093/pasj/64.6.136

[18] M. J. Reid, K. M. Menten, A. Brunthaler, X. W. Zheng, T. M. Dame, Y. Xu, Y. Wu, B. Zhang, et al., "Trigonometric parallaxes of high mass star forming regions: The structure and kinematics of the milky way," *The Astrophysical Journal*, vol. 783, no. 2, p. 130, 2014. https://doi.org/10.1088/0004-637X/783/2/130

[19] A. S. Rastorguev, N. D. Utkin, M. V. Zabolotskikh, A. K. Dambis, A. T. Bajkova, and V. V. Bobylev, "Galactic masers: Kinematics, spiral structure and the disk dynamic state," *Astrophysical Bulletin*, vol. 72, no. 2, pp. 122–140, 2017. https://doi.org/10.1134/S1990341317020043

[20] M. J. Reid, K. M. Menten, A. Brunthaler, X. W. Zheng, T. M. Dame, Y. Xu, J. Li, N. Sakai, et al., "Trigonometric parallaxes of high-mass star-forming regions: Our view of the milky way," *The Astrophysical Journal*, vol. 885, no. 2, p. 131, 2019. https://doi.org/10.3847/1538-4357/ab4a11

[21] VERA Collaboration, T. Hirota, T. Nagayama, M. Honma, Y. Adachi, R. A. Burns, J. O. Chibueze, et al., "The first VERA astrometry catalog," *Publications of the Astronomical Society of Japan*, vol. 72, no. 4, p. 50, 2020. https://doi.org/10.1093/pasj/psaa018

[22] Gaia Collaboration, S. A. Klioner, L. Lindegren, F. Mignard, J. Hernández, M. Ramos-Lerate, U. Bastian, M. Biermann, A. Bombrun, et al., "Gaia early data release 3: The celestial reference frame (Gaia-CRF3)," *Astronomy & Astrophysics*, vol. 667, p. A148, 2022.

[23] N. Liu, Z. Zhu, and J.-C. Liu, "Secular aberration drift in stellar proper motions: An additional term due to the change in line-of-sight direction," *Astronomy & Astrophysics*, vol. 688, p. L24, 2024. https://doi.org/10.1051/0004-6361/202451053

[24] A. G. A. Brown, U. Bastian, and S. Klioner, "The Gaia astrometric catalogue and secular aberration drift in proper motions," *Astronomy & Astrophysics*, vol. 695, p. A272, 2025. https://doi.org/10.1051/0004-6361/202452459

[25] O. Titov and S. Lambert, "Improved VLBI measurement of the solar system acceleration," *Astronomy & Astrophysics*, vol. 559, p. A95, 2013. https://doi.org/10.1051/0004-6361/201321806

[26] M. H. Xu, G. L. Wang, and M. Zhao, "The solar acceleration obtained by VLBI observations," *Astronomy & Astrophysics*, vol. 544, p. A135, 2012. https://doi.org/10.1051/0004-6361/201219593

[27] D. S. MacMillan, "Determination of galactic aberration from VLBI measurements and its effect on VLBI reference frames and earth orientation parameters," in *AGU Fall Meeting Abstracts*, San Francisco, California, 2014, conference abstract.

[28] O. Titov and H. Krásná, "Measurement of the solar system acceleration using the earth scale factor," *Astronomy & Astrophysics*, vol. 610, p. A36, 2018. https://doi.org/10.1051/0004-6361/201731901

[29] D. S. MacMillan, K. D. Baver, S. Bolotin, J. M. Gipson, D. Gordon, N. Habana, K. Le Bail, and L. Petrov, "GSFC VLBI Analysis Center Report," in *International VLBI Service for Geodesy and Astrometry 2019+2020 Biennial Report*, D. Behrend, K. L. Armstrong, and K. D. Baver, Eds. National Aeronautics and Space Administration, pp. 216–220, 2021, nASA/TP-20210021389.

[30] J. Böhm, S. Böhm, J. Boisits, A. Girdiuk, J. Gruber, A. Hellerschmied, H. Krásná, D. Landskron, M. Madzak, D. Mayer, J. McCallum, L. McCallum, M. Schartner, and K. Teke, "Vienna VLBI and satellite software (VieVS) for geodesy and astrometry," *Publications of the Astronomical Society of the Pacific*, vol. 130, no. 986, 2018.

[31] P. Charlot, "Radio-source structure in astrometric and geodetic very long baseline interferometry," *The Astronomical Journal*, vol. 99, pp. 1309–1326, 1990. https://doi.org/10.1086/115419

[32] J. M. Anderson and M. H. Xu, "Source structure and measurement noise are as important as all other residual sources in geodetic VLBI combined," *Journal of*

Geophysical Research: Solid Earth, vol. 123, no. 11, pp. 10 162–10 190, 2018. https://doi.org/10.1029/2018JB015550

[33] N. Kareinen, N. Zubko, T. Savolainen, M. H. Xu, and M. Poutanen, "Mitigating the effect of source structure in geodetic VLBI by re-weighting observations using closure delays and baseline-to-jet orientation," *Journal of Geodesy*, vol. 98, no. 5, p. 38, 2024. https://doi.org/10.1007/s00190-024-01837-2

[34] H. Krásná, D. Gordon, A. de Witt, and C. S. Jacobs, "The K-band (24 GHz) celestial reference frame determined from very long baseline interferometry sessions conducted over the past 20 years," in *International Association of Geodesy Symposia*. Springer, vol. 156, pp. 195–202, 2023. https://doi.org/10.1007/1345_2023_209

[35] J.-C. Liu, N. Capitaine, S. B. Lambert, Z. Malkin, and Z. Zhu, "Systematic effect of the galactic aberration on the ICRS realization and the earth orientation parameters," *Astronomy & Astrophysics*, vol. 548, p. A50, 2012. https://doi.org/10.1051/0004-6361/201219421

[36] J. Yao, J.-C. Liu, N. Liu, Z. Malkin, Z. Zhu, I. Nurul Huda, and S. B. Lambert, "Effect of galactic aberration on earth orientation parameters: From the ICRF2 to the ICRF3," *Astronomy & Astrophysics*, vol. 665, p. A121, 2022. https://doi.org/10.1051/0004-6361/202243852

[37] R. S. Gross, "Earth rotation variations—long period," in *Treatise on Geophysics*, G. Schubert, Ed. Amsterdam: Elsevier, ch. 3.09, pp. 239–294, 2007.